

V. M. Boychuk¹, R.I. Zapukhlyak¹, R.G. Abaszade², V.O. Kotsyubynsky¹,
M.A. Hodlevsky¹, B.I. Rachiy¹, L.V. Turovska³, A.M. Dmytriv³, S.V. Fedorchenko¹

Solution combustion synthesized NiFe₂O₄ / reduced graphene oxide composite nanomaterials: morphology and electrical conductivity

¹Vasyl Stefanyk Precarpathian National University, Ivano-Frankivsk Ukraine, kotsyubynsky@gmail.com.

²Azerbaijan State Oil and Industry University, Baku, Azerbaijan, abaszada@gmail.com.

³Ivano-Frankivsk National Medical University, Ivano-Frankivsk, Ukraine lturovska@gmail.com

Ultrafine NiFe₂O₄ (T0) and NiFe₂O₄ / rGO composites have been synthesized by solution combustion method. The presence of rGO in the composite (33 wt.% (T1) or 66 wt.% (T2)) causes a decrease in the average particle size of the oxide phase from 16 to 10-11 nm with their transition to superparamagnetic with a decrease in the mixed spinel inversion degree. The S_{BET} values for T1 and T2 are 180 and 315 m²/g, respectively, decreasing to 78 and 169 m²/g after annealing in the temperature range of 200-800°C. Both micro- and small mesopores (size of 2.0-4.5 nm) have been observed for samples T2, while samples T0 and T1 are mainly mesopores. The small polaron mechanism of electrical conductivity is observed for pure spinel, when the electron hopping charge transport prevails for NiFe₂O₄ / rGO composites. It can be assumed that the GO component lowers the combustion reaction temperature and prevents particle agglomeration.

Keywords: Nickel ferrite, graphene oxide, composite, Mossbauer spectroscopy, electrical conductivity.

Received 12 September 2022; Accepted 20 December 2022.

Introduction

Solution combustion synthesis (SCS) is an inexpensive, easy-to-process, one-step, fast, and energy-efficient versatile method for producing ultrafine metal oxides using exothermic self-propagating reactions [1]. The method includes a series of stages – the formation of liquid-phase sol containing cationic complexes with organic ligands, the sol to gel transition, gel aging, xerogel formation, a xerogel with the onset of an exothermic reaction, which is the driving factor of solid-phase diffusion and oxide phase formation [2]. The main advantage of SCS is the ability to quickly obtain a correspondingly large amount of material with a large specific surface area, high porosity and structural homogeneity due to the rapid evaporation of gaseous products during combustion under conditions of homogeneity and stoichiometry of the products. The peculiarities of the synthesis make it possible to limit the temperature rise and prevent the sintering of particles,

which leads to the formation of a fine powder. Changing the reaction parameters (the ratio of the precursors, the type of organic complexant, the density and thermal conductivity of the sol, the ignition temperature, and heat) makes it possible to control the properties of materials. The type and ratio of the complexant and metal salts (mainly nitrates) are the main factors that determine the time and temperature of combustion, as well as the mode of vaporization of gases. The most popular complexants (glycine (NH₂CH₂COOH), citric acid (C₆H₈O₇), urea (CO(NH₂)₂) contain carboxylate or amine groups [3]. The advantages of glycine-based synthesis are the greater probability of diffusion-limited cluster aggregation at the stage of sol to gel transition, which leads to the formation of relatively smaller aggregates and potentially causes a decrease in the average particle size [4]. The reaction conditions affect not only the morphology, but also the crystal structure of the oxide, as well as its electrophysical and magnetic properties, which are crucially important for the further use of the obtained materials. Ultrafine

transition metal oxides with a spinel structure have attracted great attention due to a wide range of novel applications, such as magnetic drug delivery, photocatalysis, gas sensors, and electrochemical energy storage devices [5]. The implementation of the SCS method is the preparation of composite materials consisting of both spinel ferrite nanoparticles and carbon components. This approach is a promising way to improve characteristics, functionality and capabilities of the material. For example, the formation of nanosized metal oxide / reduced graphene oxide (rGO) composites as an electrode of a hybrid supercapacitor allows an increase in its electrical conductivity and an increase in the rate of surface redox reactions [6]. In this study, we have presented a one-step, fast and low temperature (below 500°C) method for synthesizing NiFe₂O₄/ rGO composite materials based on glycine-assisted SCS. The properties of the products can be tuned by varying the colloidal graphene oxide in the initial sol.

I. Experimental details

The materials used were Ni(NO₃)₂·6H₂O, Fe(NO₃)₃·9H₂O (Sigma Aldrich, 98.0 %), glycine NH₂CH₂COOH. First, the stoichiometric amount of nickel and iron nitrates at Ni/Fe molar ratio of 1:2 was dissolved in 50 mL of deionized water to form a precursor solution. An aqueous solution (50 ml) of glycine was prepared and added dropwise with continuous stirring to a solution of metal precursors at cation/fuel agent molar ratio of 1:1. The final mixture with pH=3.0-3.5 was stirred at 300 rpm for 1h at 70-80°C until excess water evaporates. An aqueous solution of ammonia was added dropwise until the precursor solution had pH = 7. After the formation of a viscous solution, drying procedure was continued until a gel was formed. The gel was placed on a hot plate, which was pre-heated to 300 °C and heated at this temperature to the point of ignition. Complex oxide/rGO composite materials were obtained under the same experimental conditions by one-pot synthesis, when a colloidal solution of graphene oxide was added to the metal salt mixture before the fuel agents. Colloidal graphene oxide was prepared according to the modified Marcano-Tour protocol [7]. Both pure ferrite (T0 sample) and NiFe₂O₄/rGO composites (mass ratio of spinel and rGO phases was 3:1 (T1 sample) and 3:2 (T2 sample), respectively) were obtained. Additional annealing at 300, 400, 500, 600 and 900°C was applied to all of the obtained materials.

X-ray diffraction patterns of the synthesized powder systems were obtained on an X-ray diffractometer XRD-7000 (Shimadzu, Japan) in Cu-Kα radiation at room temperature in the Bragg-Brentano geometry. The XRD patterns were processed using the Rietveld method (Fullproff software). The average sizes of coherent scattering regions (CSR) were calculated using the Scherrer approach.⁵⁷Fe Mössbauer spectra were obtained on an MS1104EM spectrometer (⁵⁷Co source, chromium matrix, activity about 10 mCi). Isomeric shifts were calibrated relative to α-Fe. The analysis of the Mössbauer spectra was carried out using the Univem software.

BET specific surface areas were obtained from the N₂-adsorption / desorption isotherm on a pore size analyzer

(Nova 2200e, Quantachrome Instrument Corp.). Pore size distribution was calculated from isotherms using nonlocal density functional theory (NL-DFT) according to the slit/cylindrical pore model.

The frequency dependence of electrical conductivity was studied by impedance spectroscopy (Autolab PGSTAT 12 / FRA-2) in the frequency range of 0.01-100 kHz and temperature range of 25-175 °C. Cylindrical samples with a diameter of 2.5 cm were obtained by pressing at 20 kN. Electrical conductivity was measured on samples compressed between two stainless steel electrodes in a spring-loaded sample holder. This assembly was placed in a precision temperature controlled oven at a heating rate of 1 K·min⁻¹ to establish thermodynamic equilibrium.

II. Results and discussion

The main reason for XRD studies was the identification of changes in the lattice constant and inversion degree as a result of the presence of the graphene component. XRD patterns of all obtained materials (T0, T1 and T2 initial samples) correspond to nickel ferrite NiFe₂O₄, JCPDS 22-1086, Fd3m symmetry group (Fig. 1, a,c,e). Rietveld analysis revealed the formation of a single spinel ferrite phase without any additional phase for all materials without carbon (T0 series) and with the presence of the rGO component (T1 and T2 series) obtained by annealing the initial samples. The observed changes (a decrease with increasing annealing temperature) of the lattice parameter of the obtained materials can be explained both by the transformation of the crystal structure and by the effect of rGO nanoparticles in the reaction mixture at the nucleation stage (Fig.2, a). Ni²⁺ and Fe³⁺ cations can occupy two sites (tetrahedral (A) and octahedral (B)) in the spinel structure formed by face-centered cubic oxygen sublattices. The cation distribution $(Ni_{1-\gamma}Fe_{\gamma}^{3+})_A [Ni_{\gamma}^{2+}Fe_{2-\gamma}^{3+}]_B O_4^{2-}$ is characterized by the inversion degree parameter γ as the fraction of Ni²⁺ cations in octahedral sites. In normal spinels ($\gamma = 0$), divalent cations occupy A-sites, while in inverse spinels ($\gamma = 1$), all divalent cations are located in B-sites and Fe³⁺ cations occupy tetrahedral and octahedral sites. In some cases, a partial inverse structure ($0 < \gamma < 1$) of mixed spinel can be realized when divalent and trivalent cations are distributed in both A- and B-sites. Nickel ferrite NiFe₂O₄ has properties of an inverse spinel, but a decrease in particle size and non-equilibrium synthesis conditions cause changes in the cation distribution and the formation of a mixed spinel structure [8]. The formation of a mixed structure of NiFe₂O₄ synthesized by the combustion method was observed earlier [9, 10]. In the geometric model, the probability of the formation of a certain cationic configuration depends on the cationic radius - the size of B-sites is correspondingly larger than that of tetrahedral ones, therefore, Ni²⁺ cations have thermodynamic advantages over octahedral coordination. Changes in the inversion degree were estimated from the integral intensities of the (220) and (222) XRD reflexes. An increase in I₂₂₀/I₂₂₂ for a series of T0 samples with increasing temperature corresponds to an increase in the

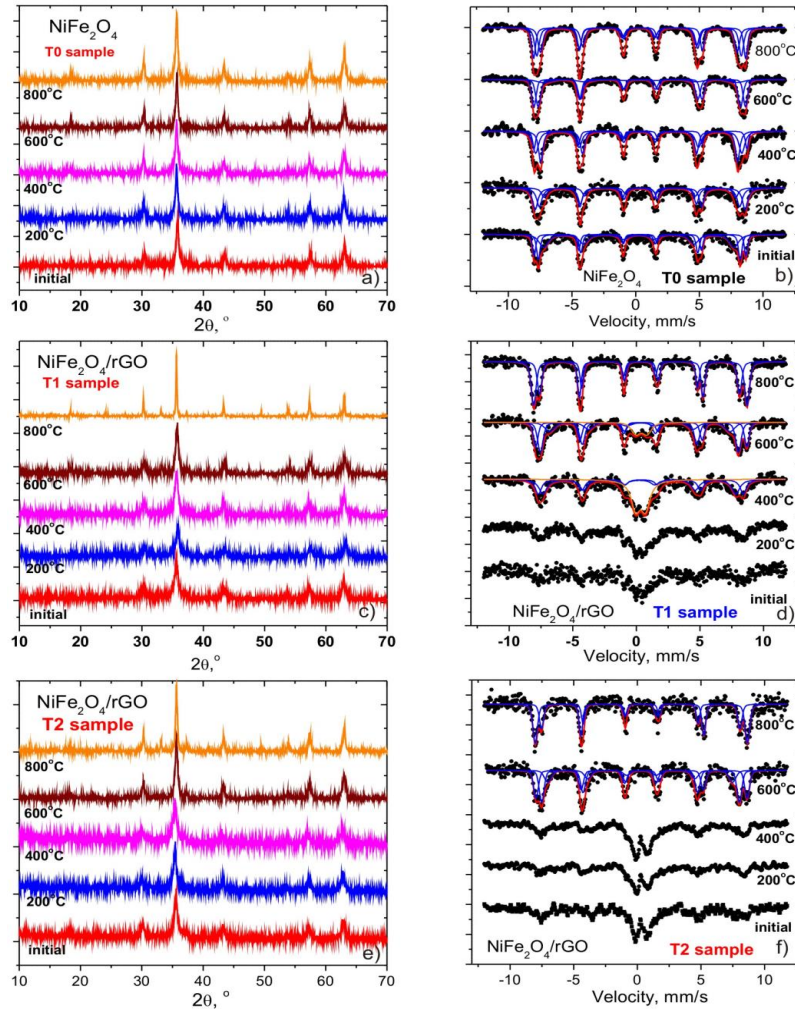


Fig. 1. Mössbauer spectra and XRD patterns of the initial and annealed nickel ferrite (sample T0) and NiFe₂O₄/rGO composites (samples T1 and T2).

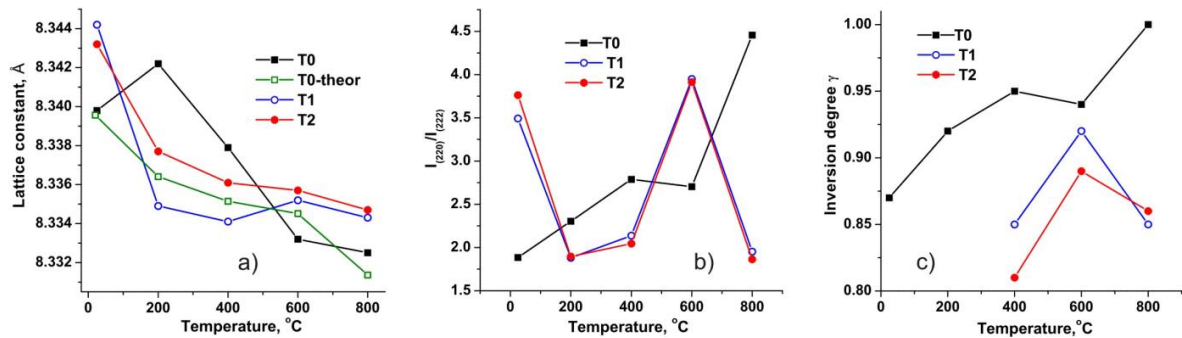


Fig. 2. (a) Lattice constant, (b) the ratio of the intensities of the (220) and (222) XRD reflexes, and (c) the inversion degree γ for T0 (pure spinel) and T1, T2 (NiFe₂O₄/rGO composites) sample series as a function of thermal treatment temperature.

inversion degree [11], when changes in I_{220}/I_{222} ratio for T1 and T2 samples are more complex (Fig. 2, b). Differences in the ionic radii of the cations cause a spatial displacement of the oxygen anions of the first coordination spheres and lead to changes in the lattice constants.

The lattice distortion degree is characterized by the parameter u , which is defined as the distance between the anions and the face of the cubic octant, in the spatial center of which the cation should be located in the absence of distortion. As a result, the radii of A- and B-sites (r_A and r_B) are calculated as:

$$r_A = \sqrt{3}\alpha(u - 1/4) - r_{O^{2-}}, \quad r_B = \alpha(5/8 - u) - r_{O^{2-}},$$

where $r_{O^{2-}} = 0.140$ nm [12].

Mössbauer spectroscopy (Fig.1, b,d,f) was used to determine the inversion degree. The experimental Mössbauer spectra were separated into individual components corresponding to Fe³⁺ ions in the A- and B-sites with different coordination numbers of magnetic neighbors in the first cationic coordination sphere. Usually A-coordinated Fe³⁺ has 12 octahedrally coordinated Fe³⁺ ions in the second coordination sphere, and each B-coordinated Fe³⁺ has 6 tetrahedrally coordinated Fe³⁺ in

neighborhood [13]. Each ion configuration corresponds to the formation of a certain type of exchange interaction, which is observed experimentally as a component of the Mössbauer spectrum. The redistribution of cations between the sublattices causes significant changes in the Mössbauer spectra. The probability of formation of certain ion configurations can be calculated as

$$P_z^{(n)} = \frac{z!}{n!(z-n)!} k^{(z-n)} (1-k)^n, \text{ where } z \text{ is the coordination}$$

number of Fe^{3+} ions ($z = 12$ for tetrahedral sites and $z = 6$ for octahedral sites), n is the number of magnetic neighbors of Fe^{3+} ions ($0 \leq n \leq z$), k is the relative amount of Ni^{2+} in the opposite sublattice. A decrease in γ has a relatively weak effect on the number of subspectra corresponding to the A-coordinated Fe^{3+} , therefore, all magnetically non-equivalent coordination can be described by only one broad magnetic sextet. At the same time, a decrease in the inverse degree leads to significant changes in the probability of the ion configuration for B-coordinated Fe^{3+} , therefore, in this case, the multiple subspectra should be used [14]. The values of isomeric shifts for tetrahedrally coordinated Fe^{3+} are relatively smaller due to stronger covalent Fe_A-O bonds, which makes it possible to identify subspectra. The calculated ratio of the integral intensities of the subspectra corresponding to tetrahedrally and octahedrally coordinated Fe^{3+} (S_A and S_B , respectively) allows calculating the inversion degree parameter as $\frac{S_A}{S_B} = \frac{f_A}{f_B} \times \frac{\gamma}{2-\gamma}$, where f_A and f_B are recoilless

f-factors of Fe^{3+} cations in the octahedral and tetrahedral sites of the $NiFe_2O_4$ structure, $f_B/f_A = 1.09 \pm 0.01$ at room temperature [8].

The estimated γ value is about 0.87 for the initial T0 sample with a gradual increase to about 1.0 with an increase in the annealing temperature (Fig.2, c). This approach for calculating the inversion degree is inapplicable for the initial and annealed at 200 and 400°C rGO-containing composite materials of T1 and T2 series due to the destruction or violation of their magnetic ordering. The Mössbauer spectra of these materials correspond to their paramagnetic properties. If the spectra of the T1-400 material contain both doublet and sextet components corresponding to the presence of paramagnetic and magnetically-ordered phases, then the next increase in the relative content of rGO in the composite leads to the complete disappearance of magnetic ordering for the T2-400 sample. The observed effects are the result of superparamagnetic relaxation, when the single domain state of ferrimagnetic particles becomes thermodynamically preferable with thermal oscillations of the magnetic moment of the particle between the easy magnetization axes of the spinel structure. A ferromagnetic particle will be observed by Mössbauer spectroscopy as paramagnetic when the average time between two flips τ_N becomes shorter than the measurement time τ_m (the lifetime of the excited state of the ^{57}Fe nucleus, $\tau_m = 141.8$ ns): $\tau_m \geq \tau_N$. The relaxation

time is calculated as $\tau_N = \tau_0 \exp\left(\frac{K_{eff} V}{kT}\right)$, where $\tau_0 = 10^{-10}$ - 10^{-11} s is the characteristic of a certain material, K_{eff} is the

effective magnetocrystalline anisotropy constant, V is the nanoparticle volume, T is the temperature. The magnitude of the magnetocrystalline anisotropy depends on the size, and for nickel ferrite with an average particle size of about 5-10 nm $K_{eff} \approx 1 \cdot 10^5$ J/m³ (Fig.3, a) [15].

The threshold value of the critical size of $NiFe_2O_4$ particles corresponding to the superparamagnetic transition, estimated for this case, is about 7.0-7.5 nm. As a result, the initial T1 and T2 samples, as well as composite materials annealed at 200°C, are formed by particles with an average size less than about 7.0-7.5 nm. Analysis of these spectra and calculation of the degree of inversion are based on the ratio of integral intensities. The inversion degree of spinel oxide component of composites annealed at 600 and 800°C is in the range of 0.81-0.91 due to lattice distortion as a result of the presence of graphene fragments. The geometric model allows the calculation of the spinel lattice constant [16, 17]:

$$\alpha_{th} = \frac{8}{3\sqrt{3}} [(r_A + r_O) + \sqrt{3}(r_B + r_O)],$$

where r_A , r_B and $r_O = 0.138$ nm are the radii of A- and B-sites and oxygen anions, respectively. The values of r_A and r_B are estimated as:

$$r_A = ((1 - \gamma) \cdot r(Ni_A^{2+}) + \gamma \cdot r(Fe_A^{3+})).$$

and

$$r_B = \frac{1}{2} (\gamma \cdot r(Ni_B^{2+}) + (2 - \gamma) \cdot r(Fe_B^{3+})),$$

where cation radii in A- and B-sites are $r(Ni_A^{2+}) = 0.0565$ nm, $r(Ni_B^{2+}) = 0.069$ nm, $r(Fe_A^{3+}) = 0.0485$ nm, $r(Fe_B^{3+}) = 0.0645$ nm.

Decrease in the inversion degree should lead to a linear increase in the lattice constant of nickel ferrite. The theoretical calculation of the lattice constant of the spinel of the T0 series was carried out using the corresponding values of inversion degree (Fig. 2, a; T0-theor curve). The Rietveld analysis of the full width of XRD reflexes and the Scherrer equation make it possible to calculate the average size of the coherent scattering region (D), which is close to the size of the ferrite particles (Fig.3, a). The initial T0 is characterized by a value of $D \approx 16$ nm, which is significantly higher compared to the initial materials of the T1 and T2 series (10.5 and 11.0 nm, respectively). An increase in the annealing temperature has a relatively weak effect on the particle size of the material T0, and at annealing temperatures of 600-800°C causes a sharp increase in the particle size of T1 and T2.

The morphology of the obtained materials was studied by the low-temperature nitrogen adsorption method. The calculation of the pore size distribution was carried out using the NL-DFT formalism in the slit-like pore approximation, which is typical for the analysis of graphene-containing materials.

The adsorption-desorption isotherms for the initial T0, T1 and T2 samples correspond to type IV, which involves reversible polymolecular adsorption by mesoporous structure (Fig. 4, a,b,c). The hysteresis loops are of the H3 type (especially for the T1 sample), which corresponds to the presence of slit-like pores [18]. The transformation of the hysteresis loop from H3 to H2, observed for the initial T2 sample, corresponds to the

formation of a spatial network consisting of both slit-like and bottleneck pores that block the desorption process [19]. As a result of annealing, the adsorption-desorption isotherms reflect the evolution of the structural and morphological characteristics of the obtained material. For pure spinel (T0 series) without a carbon component, annealing causes a shift in the starting point of capillary condensation towards higher values of p/p_0 , which implies the degradation of the porous structure with a simultaneous increase in the average size of mesopores. This is consistent with the pore size distribution (Fig.4, d) - even if the microporous component is present in the initial T0 sample, annealing at 400°C causes a rapid decrease in porosity, which is reflected in a decrease in the specific surface area (Fig.3, b).

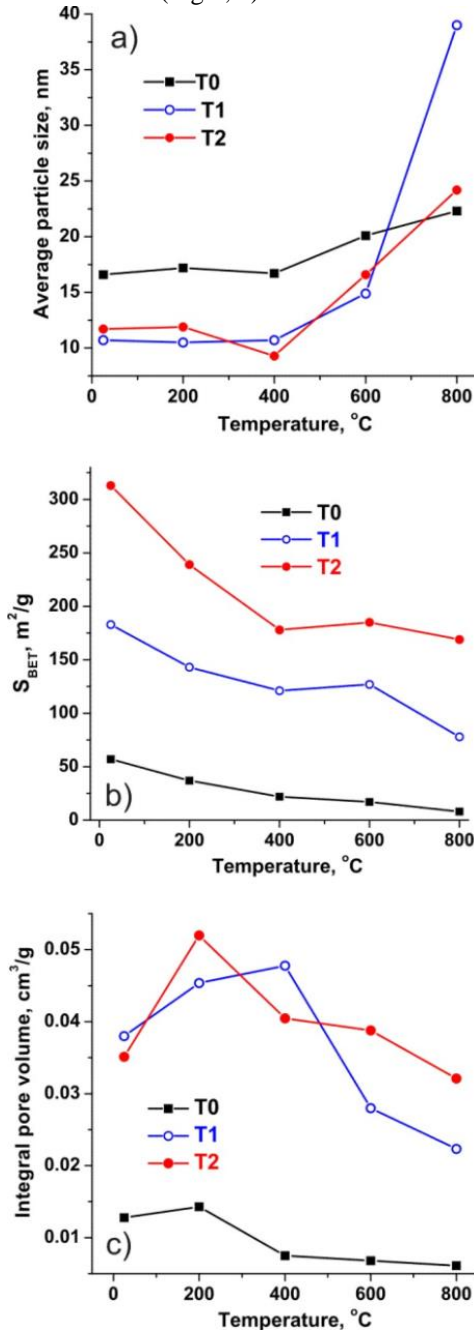


Fig 3. (a) Average particle size, (b) BET specific surface area and (c) integral pore volume of T0 (pure spinel) and T1, T2 (NiFe₂O₄/rGO composites) series depending on thermal treatment temperature.

NiFe₂O₄ / rGO composite materials have a complex porous structure with the presence of a microporous component (Fig.4, e). Annealing causes a positive shift in the broad pore size distribution for T1 series samples, with a decrease in specific surface area from about 180 m²/g for the initial T1 sample to 70 m²/g for the T1-800 material. The pore size distribution for T2 sample series is narrower (mesopore size less than 8 nm, the most likely value is 4-5 nm) with the presence of micropores (Fig.4, f).

The ratio of the volumes of micro- and mesopores weakly depends on the annealing temperature for T2 samples. The integral pore volume of both T1 and T2 sample series is approximately three times higher than the same parameter for the material without the graphene component, and also has a maximum for materials annealed at 200-400°C (Fig.3, c).

Nyquist plots (Z'' imaginary vs. Z' real) of the materials under study were measured in the frequency range of 0.01-10⁵ Hz at temperatures of 25-200°C with a step of 25°C, and the frequency dependences of the real part of the conductivity (σ) were calculated for all materials of all series (Fig.5, a, c, e). The corresponding dependences of σ on temperature were plotted at the selected frequencies (Fig.5, b, d, f).

The increase in conductivity with increasing frequency corresponds to the presence of slow polarization mechanisms, in particular, the low polaron conductivity, which is typical for spinel ferrites [20].

It is assumed that there are a strong electron-phonon interaction and charge carrier localization in relatively small volumes for a period of about 10⁻¹⁰ s [21]. The transport of highly stable small polarons in the crystal occurs as a result of thermal fluctuations with auto-localized electrons hopping between the potential minima of the crystal lattice. Under these conditions, the low mobility of small polarons causes a nonlinear dependence of the electrical conductivity on temperature with a maximum and subsequent decline. The decrease in the mobility of small polarons with increasing temperature is the result of an increase in their effective mass due to the temperature-induced growth of the phonon concentration and an increase in the number of phonons interacting with polarons. The temperature dependence of the hopping polaron conductivity is described as

$$\sigma = \frac{ne^2 a^2 \omega_0}{kT} \exp\left[-\frac{E_a}{kT}\right],$$

where n is the concentration of

polarons, a is the interionic distance, e is the electron charge, ω_0 is the frequency of optical phonons, E_a is the activation energy of the polaron hopping transport, k is the Boltzmann constant.

The activation energy E_a of small polaron traps was estimated from the linear approximation of the $\ln(\sigma T) = f(1/T)$ plots (Fig.6, a). It was found that the frequency dependence $E_a(\omega)$ has a maximum (0.19 eV) at 10 Hz, while at low frequencies (0.01-0.1 Hz), the E_a values are lower (about 0.165 eV).

The minimum values of E_a (up to 0.12 eV) for the T0 material were observed at a high frequency (Fig.6, c). The presence of the graphene component in the materials of the T1 and T2 series leads to a change in the charge transport conditions. Changes in the conductivity of rGO in the

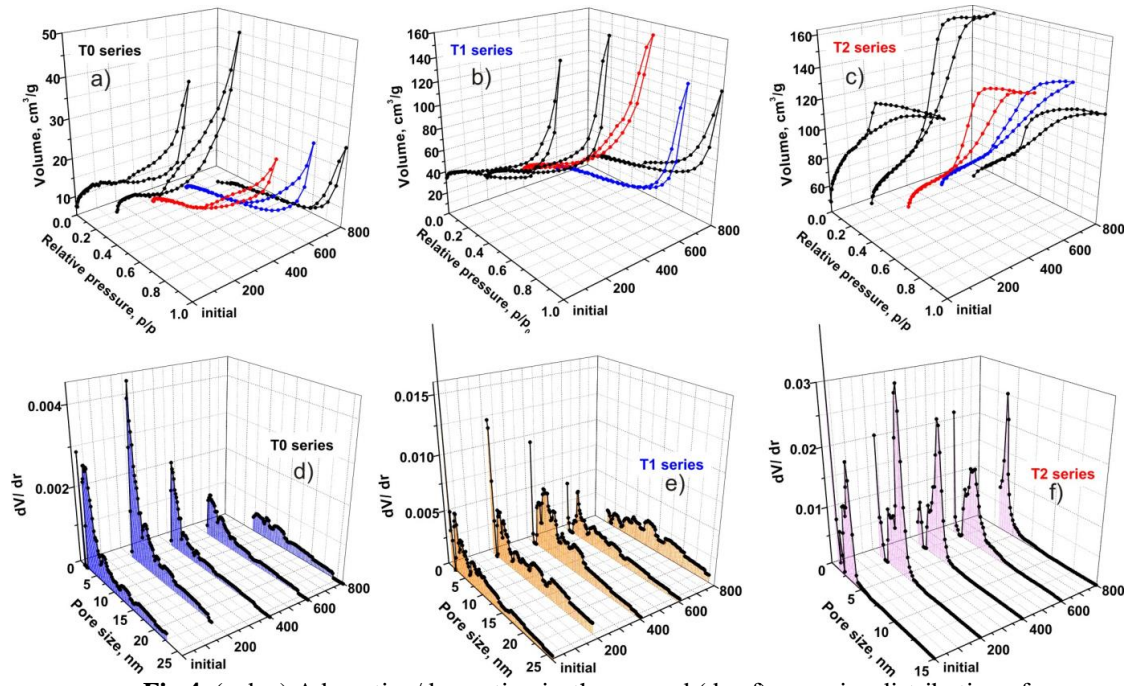


Fig.4. (a, b,c) Adsorption/desorption isotherms and (d,e, f) pore size distribution of T0 (pure spinel) and T1, T2 (NiFe₂O₄/rGO composites) sample series .

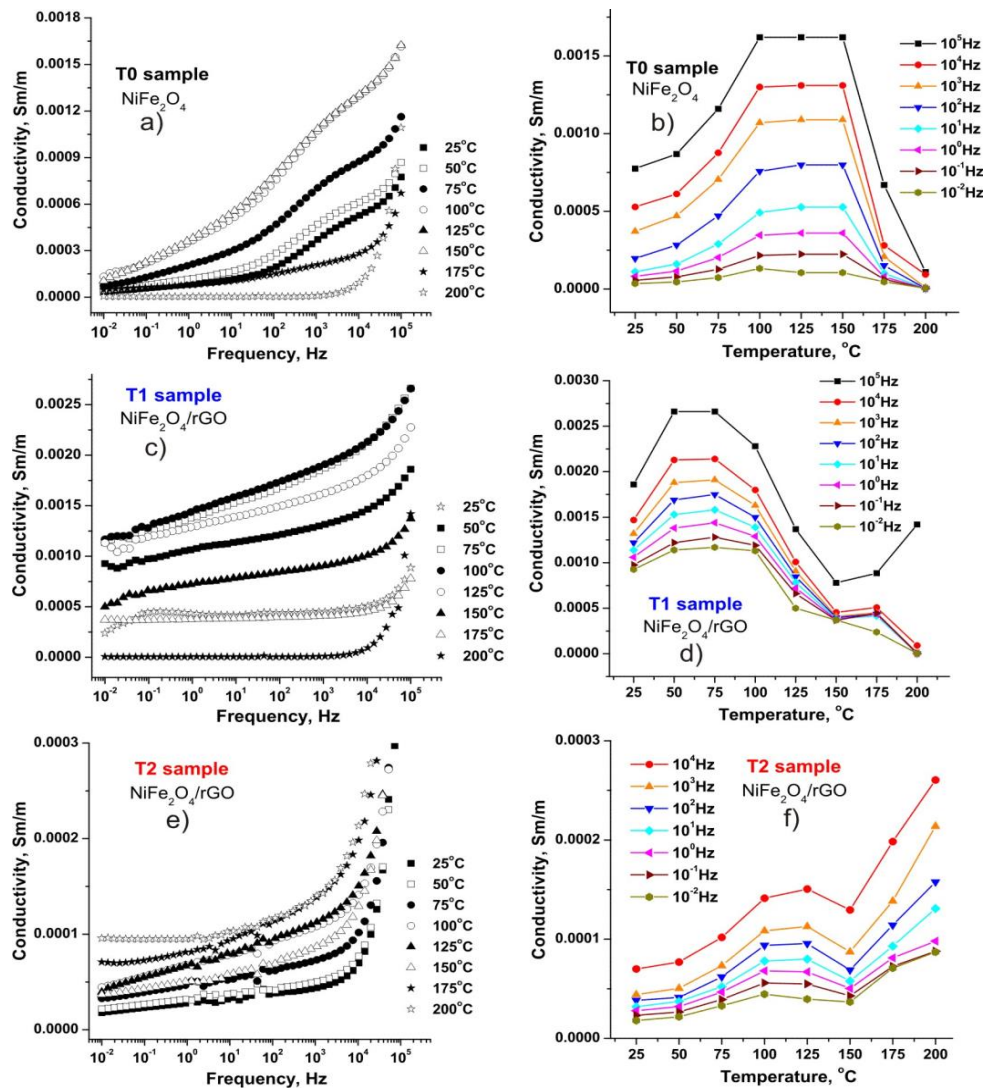


Fig.5. (a,c,e) Electrical conductivity spectra and (b, d, f) temperature dependences of electrical conductivity of T0 (pure spinel) and T1, T2 (NiFe₂O₄ / rGO composites) sample series.

temperature range of 25-110 K correspond to the Efros-Shklovskii variable-range-hopping (ES-VRH) charge transport [22] and in some cases, this mechanism is observed up to room temperature [23], but at temperatures > 200 K, Arrhenius transport mechanism is typical [24]. Additional information was obtained from the frequency dependence of σ . An increase in the relative content of rGO for the initial T2 sample leads to a transformation of the conductivity spectra to the Jonscher-type (a low change of the AC conductivity at low frequencies and a sharp increase with increasing frequency), which corresponds to hopping charge transport in disordered materials [6]:

$\sigma(f) = \sigma_{dc} \left[1 + (f/f_h)^n \right]$, where σ_{dc} is the DC conductivity, f_h is the hopping frequency of charge carriers, n is the frequency exponent parameter, n is the degree of connectedness of the charge trapping pathways, and in the

general case, this parameter ranges from 0 to 1 [25]. The dependence $\sigma(f)$, measured in temperature range of 25-200°C for the initial T2 sample, was consistent with Jonscher's equation (Fig. 7, a). It can be assumed that the temperature dependence of the electrical conductivity of T1 and T2 reflects the presence of several types of hopping mechanisms. Assuming the predominance of the Arrhenius mechanism for the initial T2 sample (Fig.6, b), the values of the activation energy were calculated (Fig.6, c). The approximation errors for the parameters ω_h and n did not exceed 15% of the absolute value with the adjusted R-squared > 0.956.

It was found that the carrier hopping frequency varies in the range of 7–11 kHz, acquiring a local maximum at a measurement temperature in the range of 75–100°C (Fig. 7, b). The initial T1 sample with relatively low rGO content has intermediate properties, which makes it impossible to adequately approximate it. The observed

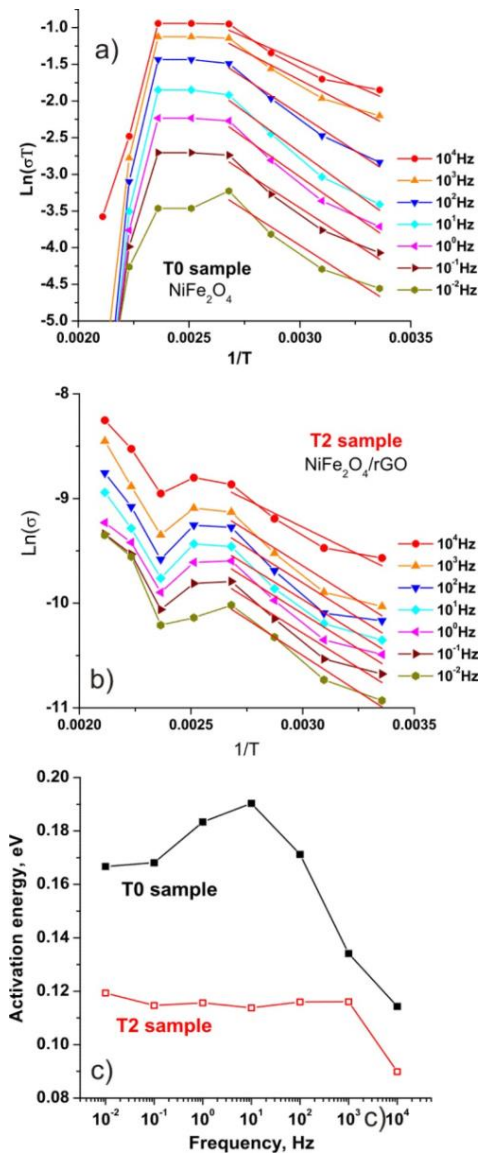


Fig. 6. Plots of (a) $\ln(\sigma T)$ vs. $1/T$ and (b) $\ln(\sigma)$ vs. $1/T$ for the initial T0 and T2 samples with linear fitting and (c) the corresponding values of the hopping activation energy as a function of frequency.

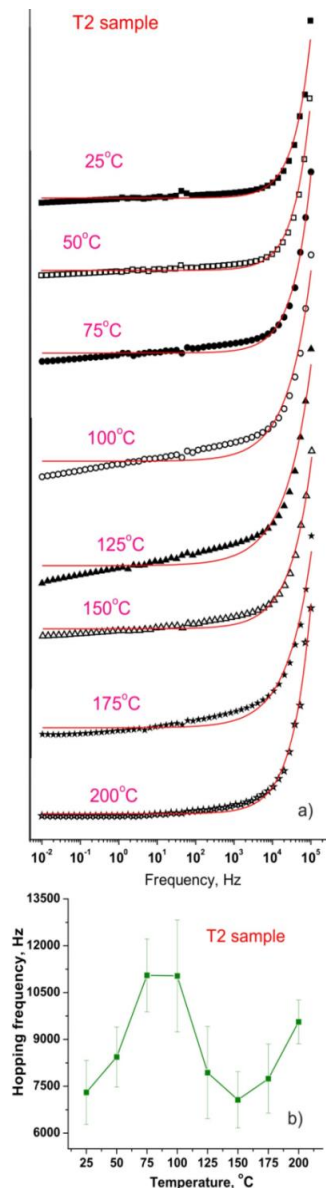


Fig. 7. (a) Electrical conductivity spectra measured for the initial T2 sample (NiFe₂O₄ / rGO composites), solid lines best fit the experimental data using Jonscher's formula, and (b) corresponding temperature dependence of the charge carrier hopping frequency.

patterns of structural, morphological, and electrophysical properties of the obtained materials can be generalized using the following model. The initial T0 material is a mesoporous system of weakly agglomerated nickel ferrite particles with an average size of about 15 nm with frequency-dependent electrical conductivity in accordance with a small polaron mechanism. The initial T1 material is a system of oxide particles with a spinel structure forming a mesoporous network partially filled with rGO fragments. Electron transport is realized as both the small polaron transport and electron hopping between rGO particles. The initial T2 material can be described as a system in which spinel particles are covered by a shell of reduced graphene oxide particles. In this case, the hopping mechanism of electron transport is realized in a network of weakly contacting carbon fragments, which explains both the lower activation energy and its weak frequency dependence.

Conclusion

NiFe₂O₄/ reduced graphene oxide (rGO) composites have been synthesized by solution combustion method using glycine as a fuel agent (the molar ratio of Ni : glycine was 1:1). GO has been prepared by the modified Hummers method. Both pure ferrite (T0 sample) and NiFe₂O₄/ rGO composites (mass ratio of spinel and rGO phases was 3:1 (T1 sample) and 3:2 (T2 sample)) have been obtained. Thermal reduction of GO has been carried out by self-propagating autocombustion. The effect of the amount of rGO component and additional thermal treatment on the phase composition, oxide particle size, and magnetic properties has been characterized by XRD, low-temperature nitrogen adsorption method, Mössbauer and impedance spectroscopy. An increase in the rGO content causes a decrease in the particles size from 15-18 nm for T0 to about 10-11 and 6-8 nm for T1 and T2 samples, respectively, with a simultaneous decrease in the inversion degree of (Ni²⁺_{1-x}Fe³⁺_x)[Ni²⁺_xFe³⁺_{2-x}]O₄ mixed spinel. The

Mössbauer spectra of T1 sample consist of a central doublet and a broadened sextet, which corresponds to the presence of both ferromagnetic and superparamagnetic ferrite particles, when the spectra for T2 sample indicate the transition of all particles to a single-domain superparamagnetic state. The BET isotherms of composite samples correspond to type IV adsorption with predominant mesopores. The specific surface areas of T0, T1 and T2 samples were 28, 125 and 152 m²/g, respectively. A small polaron mechanism of electrical conductivity (frequency-dependent activation energy in the range of 0.12-0.19 eV) has been observed for T0 material. Electron hopping charge transport (frequency-dependent activation energy in the range of 0.09-0.12 eV, hopping frequency in the range of 7–11 kHz) dominates for T2 sample when the T1 material combines two conductivity mechanisms. An increase in the rGO content causes the formation of a system of spinel particles covered with reduced graphene oxide particles. The use of the GO component in the solution combustion synthesis makes it possible to reduce the combustion reaction temperature and prevent particle sintering with an increase in the electrical conductivity of the composite material

Acknowledgments

The work was funded by the National Research Foundation of Ukraine (2020.02 / 0043).

Boychuk V.M. – professor, Doctor of Physical and Mathematical Sciences;
Zapukhlyak R.I. – PhD, Senior Researcher;
Abaszade R.G. – Associate professor, PhD;
Kotsyubynsky V.O. – Doctor of Physical and Mathematical Sciences, professor;
Hodlevsky M.A. – aspirant;
Rachiy B.I. – Doctor of Physical and Mathematical Sciences, professor;
Turovska L.V. – Associate professor, PhD;
Dmytriv A.M. – Associate professor, PhD;
Fedorchenko S.V. – Associate professor, PhD.

- [1] E. Carlos, R. Martins, E. Fortunato, R. Branquinho, *Frontispiece: Solution Combustion Synthesis: Towards a Sustainable Approach for Metal Oxides*, Chemistry – A European Journal, 26, 9099 (2020); <https://doi.org/10.1002/chem.202084264>
- [2] A. Varma, A. S. Mukasyan, A. S. Rogachev, K. V. Manukyan, *Solution combustion synthesis of nanoscale materials*, Chem. Rev., 116, 14493 (2016); <https://doi.org/10.1021/acs.chemrev.6b00279>.
- [3] A. Sutka, G. Mezinskis, *Sol-gel auto-combustion synthesis of spinel-type ferrite nanomaterials*, Frontiers of Materials Science, 128, 6 (2012); <https://doi.org/10.1007/s11706-012-0167-3>.
- [4] V. Boychuk, V. Kotsyubynsky, Kh. Bandura, I. Yaremiy, R. Zapukhlyak, S. Fedorchenko, *Self-combustion synthesized NiFe₂O₄/ reduced graphene oxide composite nanomaterials: Effect of chelating agent type on the crystal structure and magnetic properties*, Mater. Today: Proc., 35, 542 (2021); <https://doi.org/10.1016/j.matpr.2019.10.026>.
- [5] S. B. Narang, K. Pubby, *Nickel spinel ferrites: a review*, J. Magn. Mater., 519, 167 (2021); <https://doi.org/10.1016/j.jmmm.2020.167163>.
- [6] V.M. Boychuk, V.O. Kotsyubynsky, K.V. Bandura, B.I. Rachii, I.P. Yaremiy, S.V. Fedorchenko, *Structural and electrical properties of nickel-iron spinel/reduced graphene oxide nanocomposites*, Mol. Cryst. Liq. Cryst., 673, 137 (2019); <https://doi.org/10.1080/15421406.2019.1578503>.
- [7] V. O. Kotsyubynsky, V. M. Boychuk, I. M. Budzulyak, B. I. Rachiy, M. A. Hodlevska, A. I. Kachmar, M.A. Hodlevsky, *Graphene oxide synthesis using modified Tour method*, Adv. Nat. Sci.: Nanosci. Nanotechnol., 12, 035006 (2021); <https://doi.org/10.1088/2043-6262/ac204f>.

- [8] H. Salazar-Tamayo, K. E. García, C. A. Barrero, *New method to calculate Mössbauer recoilless f-factors in NiFe₂O₄ Magnetic, morphological and structural properties*, J. Magn. Magn. Mater., 471, 242 (2019); <https://doi.org/10.1016/j.jmmm.2018.09.066>.
- [9] R. S. Yadav, I. Kuřitka, J. Vilcakova, J. Havlica, J. Masilko, L. Kalina, M. Hajdúchová, *Structural, magnetic, dielectric, and electrical properties of NiFe₂O₄ spinel ferrite nanoparticles prepared by honey-mediated sol-gel combustion*, J. Phys. Chem. Solids, 107, 150 (2017); <https://doi.org/10.1021/acsomega.9b03191>.
- [10] R. Tiwari, M. De, H. S. Tewari, & S. K. Ghoshal, *Structural and magnetic properties of tailored NiFe₂O₄ nanostructures synthesized using auto-combustion method*, Results Phys., 16, 102916 (2020); <https://doi.org/10.1016/j.rinp.2019.102916>.
- [11] M. Mozaffari, M. E. Arani, & J. Amighian, *The effect of cation distribution on magnetization of ZnFe₂O₄ nanoparticles*, J. Magn. Magn. Mater, 322, 3240 (2010); <https://doi.org/10.1109/TMAG.2015.2440478>.
- [12] R. D. Shannon, *Revise deffective ionic radii and systematic studies of interatomic distances in halides and chalcogenides*, Acta Cryst, 32, 751 (1976); <https://doi.org/10.1107/S0567739476001551>.
- [13] V. Kotsyubynsky, B. Ostafiychuk, V. Moklyak, A. Hrubciak, *Synthesis, characterization and electrochemical properties of mesoporous maghemite γ -Fe₂O₃*, In Solid State Phenomena, 230, 120 (2015); <https://doi.org/10.4028/www.scientific.net/SSP.230.120>.
- [14] T. Tatarchuk, N. Danyliuk, A. Shyichuk, V. Kotsyubynsky, I. Lapchuk, V. Mandzyuk, *Green synthesis of cobalt ferrite using grape extract: the impact of cation distribution and inversion degree on the catalytic activity in the decomposition of hydrogen peroxide*, Emergent Mater., 1 (2021); <https://doi.org/10.1007/s42247-021-00323-1>.
- [15] S. Mitra, K. Mandal, & P. A. Kumar, *Temperature dependence of magnetic properties of NiFe₂O₄ nanoparticles embeded in SiO₂ matrix*, J. Magn. Magn. Mater, 306, 254 (2006); <https://doi.org/10.1016/j.jmmm.2006.03.024>.
- [16] B. V. Prasad, B. R. Babu, M. S. R. Prasad, *Structural and dielectric studies of Mg²⁺ substituted Ni-Zn ferrite*, Mater. Sci.-Pol., 33, 806 (2015); <https://doi.org/10.1515/msp-2015-0111>.
- [17] H. Salazar-Tamayo, K. E. G. Tellez, C. A. B. Meneses, *Cation Vacancies in NiFe₂O₄ During Heat Treatments at High Temperatures: Structural, Morphological and Magnetic Characterization*, Mat. Res., 22, 0298 (2019); <https://doi.org/10.1590/1980-5373-mr-2019-0298>.
- [18] M. Thommes, K. Kaneko, A. V. Neimark, J. P. Olivier, F. Rodriguez-Reinoso, J. Rouquerol, K. S. Sing, *Physisorption of gases, with special reference to the evaluation of surface area and pore size distribution (IUPAC Technical Report)*, Pure Appl. Chem., 87, 1051 (2015); <https://doi.org/10.1515/pac-2014-1117>.
- [19] K. S. Sing, R. T. Williams, *Physisorption hysteresis loops and the characterization of nanoporous materials*, Adsorption Science & Technology, 22, 773 (2004); <https://doi.org/10.1260/0263617053499032>.
- [20] M. Younas, M. Nadeem, M. Atif, R. Grossinger, *Metal-semiconductor transition in NiFe₂O₄ nanoparticles due to reverse cationic distribution by impedance spectroscopy*, J. Appl. Phys., 109, 093704 (2011); <https://doi.org/10.1063/1.3582142>.
- [21] Z. Ž. Lazarević, Č. Jovalekić, A. Milutinović, D. Sekulić, V. N. Ivanovski, A. B. Rečnik, Ž. Cekić, N. Romčević, *Nanodimensional spinel NiFe₂O₄ and ZnFe₂O₄ ferrites prepared by soft mechanochemical synthesis*, J. Appl. Phys., 113, 187221 (2013); <https://doi.org/10.1063/1.4801962>.
- [22] A. Bhaumik, J. Narayan, *Conversion of p to n-type reduced graphene oxide by laser annealing at room temperature and pressure*, Journal of Applied Physics, 121, 125303 (2017); <https://doi.org/10.1063/1.4979211>.
- [23] Joung, D., Khondaker, S. I., “Efros-Shklovskii variable-range hopping in reduced graphene oxide sheets of varying carbon s p² fraction”, *Phys. Rev. B*, 86(2012), 235423 <https://doi.org/10.1103/PhysRevB.86.235423>
- [24] A. Haque, M. Abdullah-Al Mamun, M. F. N. Taufique, P. Karnati, K. Ghosh, *Large magnetoresistance and electrical transport properties in reduced graphene oxide thin film*, IEEE Trans. Magn., 54, 1 (2018); <https://doi.org/10.1109/TMAG.2018.2873508>.
- [25] J. C. Dyre, T. B. Schrøder, *Universality of ac conduction in disordered solids*, Rev. Mod. Phys., 72, 873(2000); <https://doi.org/10.1103/RevModPhys.72.873>.

В. М. Бойчук¹, Р.І. Запукхляк¹, Р.Г. Абасзаде², В.О. Коцюбинський¹,
М.А. Годлевський¹, Б.І. Рачій¹, Л.В. Туровська³, А.М. Дмитрів³, С.В. Федорченко¹

Нанокompозит NiFe₂O₄ / відновлений оксид графену отриманий методом золь-гель автогоріння: морфологічні та електричні властивості

¹Прикарпатський національний університет імені Василя Стефаника, Івано-Франківськ, Україна,
kotsyubynsky@gmail.com

²Азербайджанський державний університет нафти і промисловості, Баку, Азербайджан, abaszada@gmail.com

³Івано-Франківський національний медичний університет, Івано-Франківськ, Україна lturovska@gmail.com

Методом золь-гель автогоріння отримано ультрадисперсні композити NiFe₂O₄ (T0) і NiFe₂O₄ / rGO. Наявність rGO в композиті (33 мас. % (T1) або 66 мас. % (T2)) зумовлює зменшення середнього розміру частинок оксидної фази з 16 до 10-11 нм з переходом їх у суперпарамагнітний стан зі зниження ступеня інверсії фази змішаної шпінелі NiFe₂O₄. Значення SBET для матеріалів T1 і T2 становлять 180 і 315 м²/г відповідно, зменшуючись до 78 і 169 м²/г після відпалу в діапазоні температур 200-800°C. Для зразка T2 спостерігаються як мікро-, так і малі мезопори (розмір 2,0-4,5 нм), тоді як зразки T0 і T1 є переважно мезопористими. Для чистої шпінелі T0 домінує механізм електропровідності, базований на транспорті малих поляронів, в той час як композитів NiFe₂O₄ / rGO переважає стрибковий транспорт заряду електронів. Встановлено, що присутність компоненти оксиду графену знижує температуру реакції горіння та запобігає агломерації частинок оксидної фази.

Ключові слова: оксид графену, нанокompозит, нікелевий ферит, месбауєрівська спектроскопія, електрична провідність.